Intelligent control strategy for electrified pressure-swing distillation processes using artificial neural networks-based composition controllers

Yang, Daye; Wang, Jingcheng; Cai, Huihuang; Rao, Jun; Cui, Chengtian

DOI
10.1016/j.seppur.2024.130991

Publication date
2025

Document Version
Final published version

Published in
Separation and Purification Technology

Separation and Purification Technology 360 (2025) 130991

Contents lists available at ScienceDirect

Separation and Purification Technology

journal homepage: www.elsevier.com/locate/seppur

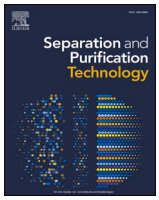

Intelligent control strategy for electrified pressure-swing distillation processes using artificial neural networks-based composition controllers

Daye Yang [a], Jingcheng Wang [a,*], Huihuang Cai [a], Jun Rao [a], Chengtian Cui [b,*]

[a] Department of Automation, Key Laboratory of System Control and Information Processing, Shanghai Jiao Tong University, Shanghai 200240, PR China
[b] Department of Chemical Engineering, Delft University of Technology, Van der Maasweg 9, Delft 2629 HZ, the Netherlands

ARTICLE INFO

Editor: Dr. B. Van der Bruggen

Keywords:
Pressure-swing distillation
Electrically-driven process
Artificial neural networks
Intelligent composition control
Dynamics and control

ABSTRACT

This study introduces a novel artificial neural network (ANN)-based control strategy for pressure-swing distillation (PSD) systems, integrating heat pump-assisted distillation (HPAD) and self-heat recuperation technology (SHRT) to transition from thermally-driven to electrically-driven processes. While previous research has validated the dynamics and controllability of conventional PSD (PSD-CONV), PSD-HPAD, and PSD-SHRT for separating a maximum-boiling acetone/chloroform azeotrope, this work specifically focuses on enhancing product purity control through composition-temperature cascade control (CC-TC). Although similar control strategies have been proposed, our approach uniquely predicts temperature set points using easily measurable process variables, effectively bypassing the inaccuracies of composition measurements. Simulation results demonstrate that this ANN-based strategy significantly improves dynamic performance and adaptability in controlling product purity without requiring a composition analyzer. By leveraging the strengths of traditional Proportional-Integral-Derivative (PID) control alongside data-driven methods, this research highlights a critical advancement in the control of electrified PSD applications, paving the way for more efficient and reliable distillation processes.

1. Introduction

Distillation remains the leading method used in various industries for the separation and purification of condensable mixtures. However, its thermal inefficiency leads to significant energy consumption and carbon dioxide emissions from fossil fuels. To address this, electrification is increasingly favored to reduce carbon emissions by using electricity from renewable resources [1–3]. As the chemical industry evolves, there is growing demand for advancements in distillation technology, driven by the need for high product quality and the complexities introduced by azeotropes. This has led to the development of specialized techniques like pressure swing distillation (PSD) [4–6], extractive distillation (ED) [7–9], and heterogeneous azeotropic distillation (HAD) [10,11]. Azeotropes are mixtures in which the liquid and vapor phases have identical compositions [12]. They can generally be classified into minimum-boiling and maximum-boiling types, although some exhibit unique minimum–maximum boiling behaviors as pressure varies [13]. Certain pressure-sensitive azeotropes can be separated using PSD, allowing high-purity product extraction from one end of the column while recycling streams close to the azeotropic point from the other. PSD has gained attention for its solvent-free operation and energy-saving potential, utilizing pressure differences to facilitate heat pump assistance and integration [14–17]. However, depending on boiling point differences, electrification via mechanical vapor recompression may offer greater energy savings than heat integration [18–20].

Most studies focused on transitioning from thermally-driven to electrically-driven PSD processes emphasize steady-state design. However, effective control strategies are essential for practical applications, facing two main challenges: first, the complex dynamics introduced by electrification [21]; second, the intermittency of renewable energy sources. For the former, integrating heat pumps complicates process design and may require additional measures like extra reboilers for stability [22]. The latter challenge involves managing the intermittency and fluctuations inherent in renewable energy sources, which can be addressed through energy storage or by implementing integrated scheduling and control strategies enhanced by predictive analytics and machine learning [1]. An effective control strategy should ideally address several key aspects, including minimizing system fluctuations, deviations in product composition, and control costs [23]. For thermally-driven PSD processes, Luyben and Chien [12] proposed several practical control strategies that include basic PI (Proportional-Integral) controllers—such as those for flow rate, pressure, liquid level,

* Corresponding authors.
E-mail addresses: jcwang@sjtu.edu.cn (J. Wang), c.cui-1@tudelft.nl (C. Cui).

https://doi.org/10.1016/j.seppur.2024.130991
Received 30 August 2024; Received in revised form 5 December 2024; Accepted 6 December 2024
Available online 8 December 2024

and temperature—which provide robust control suitable for industrial applications [24]. Building upon these control schemes, additional PI-based strategies—such as composition-temperature cascade control, pressure-compensated temperature control, and fixed reflux ratio (RR) schemes—are essential for maintaining stability in electrically-driven PSD processes [25,26]. Furthermore, insights from these studies suggest that current temperature controls struggle with precise composition management due to their nonlinear relationships, and online composition analyzers are costly and complex to maintain. This makes composition control challenging, limiting the broader implementation of electrically-driven PSD processes, an area that remains underexplored in research. Developing intelligent composition controllers that eliminate the need for expensive composition analyzers is crucial for advancing these systems. Artificial neural networks (ANNs) are increasingly recognized as a powerful data-driven approach for efficiently managing complex, high-dimensional, and nonlinear data [27,28]. Due to these capabilities, ANNs have been successfully applied across a wide range of fields, including autonomous driving, natural language processing, and medical image analysis [29–31]. In chemical processes, ANNs also offer effective solutions for addressing the challenge of unmeasurable variables in the control of distillation processes [23]. For instance, a soft sensor utilizing a recurrent neural network has been employed for real-time monitoring and precise control of n-butyl acetate production in a reactive distillation column, achieving high accuracy and low prediction error [32]. Shan et al. [33] developed a novel soft sensor model predictive control (MPC) based on time-delayed neural networks for HAD, which achieved superior product purity control without direct composition measurements compared to conventional PID (Proportional-Integral-Derivative) and MPC methods. In the context of ANN applications in PSD processes, Li et al. [10] developed a dynamic optimization control model based on ANNs for the separation of a minimum-boiling azeotrope isoamyl-alcohol/toluene in PSD processes, both with and without heat integration. By predicting optimal operating parameters in the dynamic simulations, the model effectively reduced economic costs and energy consumption. However, this work did not address the elimination of costly composition analyzers. Sun et al. [23] proposed an intelligent control strategy based on a backpropagation (BP) neural network, validating it in two typical thermally-driven triple-column PSD systems: one with minimum-boiling azeotrope (ethanol/tetrahydrofuran/water) and one with maximum-boiling azeotrope (acetonitrile/isopropanol/water). Their results demonstrated that this strategy provides excellent dynamic performance under ± 20 % feed throughput and composition disturbances, enabling effective composition control without the need for composition analyzers. In our previous work [25], we compared the dynamic behaviors of thermally-driven (using conventional reboiler steam) and electrically-driven (heat pump assisted distillation (HPAD) and self-heat recuperation technology (SHRT)) PSD processes using a maximum-boiling acetone/chloroform case. The results indicated that the controllability of the more complex electrically-driven processes is comparable to that of the conventional sequence, with PSD-CONV exhibiting even higher oscillation amplitudes than PSD-HPAD and PSD-SHRT. Nonetheless, the dynamic results suggest that there is still room for improvement in the purity of the acetone and chloroform products. Additionally, literature surveys reveal that few studies have focused on the ANN-based control strategy for electrified PSD processes, with most research predominantly addressing minimum-boiling azeotropes and thermally-driven PSD processes.

Guided by insights from previous studies, this work aims to develop an intelligent composition controller to replace the traditional PI composition control in electrified PSD configurations (PSD-HPAD and PSD-SHRT). A maximum-boiling azeotrope of acetone/chloroform is selected as a case study, where the minimal pressure-induced shift presents a greater challenge compared to more pressure-sensitive species. The significance of this work lies in achieving high-precision product purity control in energy-efficient electrified PSD processes while avoiding the use of composition measurement instruments.

2. Methodology

2.1. Steady-state process description

The normal boiling points of acetone and chloroform are 56.5 °C and 61.2 °C, respectively. Under 1 atm pressure, they form a maximum-boiling azeotrope with a composition of 34.09 mol% acetone at 64.4 °C. The feedstock is saturated liquid at 100 kmol/h with an equimolar composition. Both product streams are required to have a purity of 99.5 mol%. The Wilson thermodynamic model is used with binary interaction parameters provided in previous work [5]. The *T-x-y* and *x-y* diagrams under 10 and 0.77 bar in Fig. S1 highlight the close-boiling characteristics of the two species and the minimal composition shifts induced by pressure. Luyben's comparative study on ED and PSD showed that ED is more favorable in terms of capital investment and energy efficiency [35]. However, ED requires an additional entrainer, a drawback that PSD addresses, albeit with the trade-offs of more stages, a higher reflux ratio, and a significant recycle flowrate.

The steady-state processes for PSD-CONV, PSD-HPAD, and PSD-SHRT are given in Fig. 1. Energy recovered from the bottom effluents is used to preheat the feed streams via feed-effluent heat exchangers. In the PSD-CONV process, the reboilers of high-pressure column (HPC) and low-pressure column (LPC) are powered by middle-pressure steam (MPS) and low-pressure steam (LPS), respectively. In the PSD-HPAD process, the reboilers are powered by the pressured streams from the overhead vapor. However, a small amount of MPS and LPS is still necessary to preheat the compressor inlet stream, preventing the formation of liquid droplets in the compressors. In the PSD-SHRT process, full electrification is possible. Economically, the implementation of electrification could reduce total annual cost (TAC) by 50 % compared to the conventional stream-driven process. Environmentally, CO_2 emissions could be reduced by 85 % even when using electricity derived from fossil fuels [5]. The use of low-carbon electricity generated from renewable energy could further support industrial decarbonization efforts.

2.2. Artificial neural network

ANN underpins the intelligent control mechanisms explored in this study. As illustrated in Fig. 2, the ANN employed is a multilayer feed-forward network, which is trained using the BP algorithm. This algorithm, rooted in the gradient descent method, employs gradient search techniques to minimize the mean squared error (*MSE*) between the network's actual output and the desired output values [36]. The derivation of the BP algorithm proceeds as follows:

Consider an input layer with n variables, denoted as $X = \{x_1, x_2, x_i, \ldots, x_n\}$, where each x_i represents a distinct process variable in the electrified PSD process. The output layer variables are represented as $Y = \{y_1, y_2, y_k, \ldots, y_n\}$, which correspond to the neural network's output variables, such as product composition or the temperature controller set point in this context.

The network's architecture includes a hidden layer $H = \{h_1, h_2, h_j, \ldots, h_p\}$, with weights $\omega_{ij}^{(1)}$ and $\omega_{jk}^{(2)}$ representing the connections between the input and hidden layers, and between the hidden and output layers, respectively. Each neuron's activation function is denoted by f. Consequently, the signal propagation through the network according to the BP algorithm is expressed by the following equations:

$$h_j = f\left(\sum_{i=1}^{n} \omega_{ij}^{(1)} x_i + b_j^{(1)}\right), j = 1, 2, \ldots, p \tag{1}$$

$$y_k = f\left(\sum_{i=1}^{p} \omega_{jk}^{(2)} h_j + b_k^{(2)}\right), k = 1, 2, \ldots, m \tag{2}$$

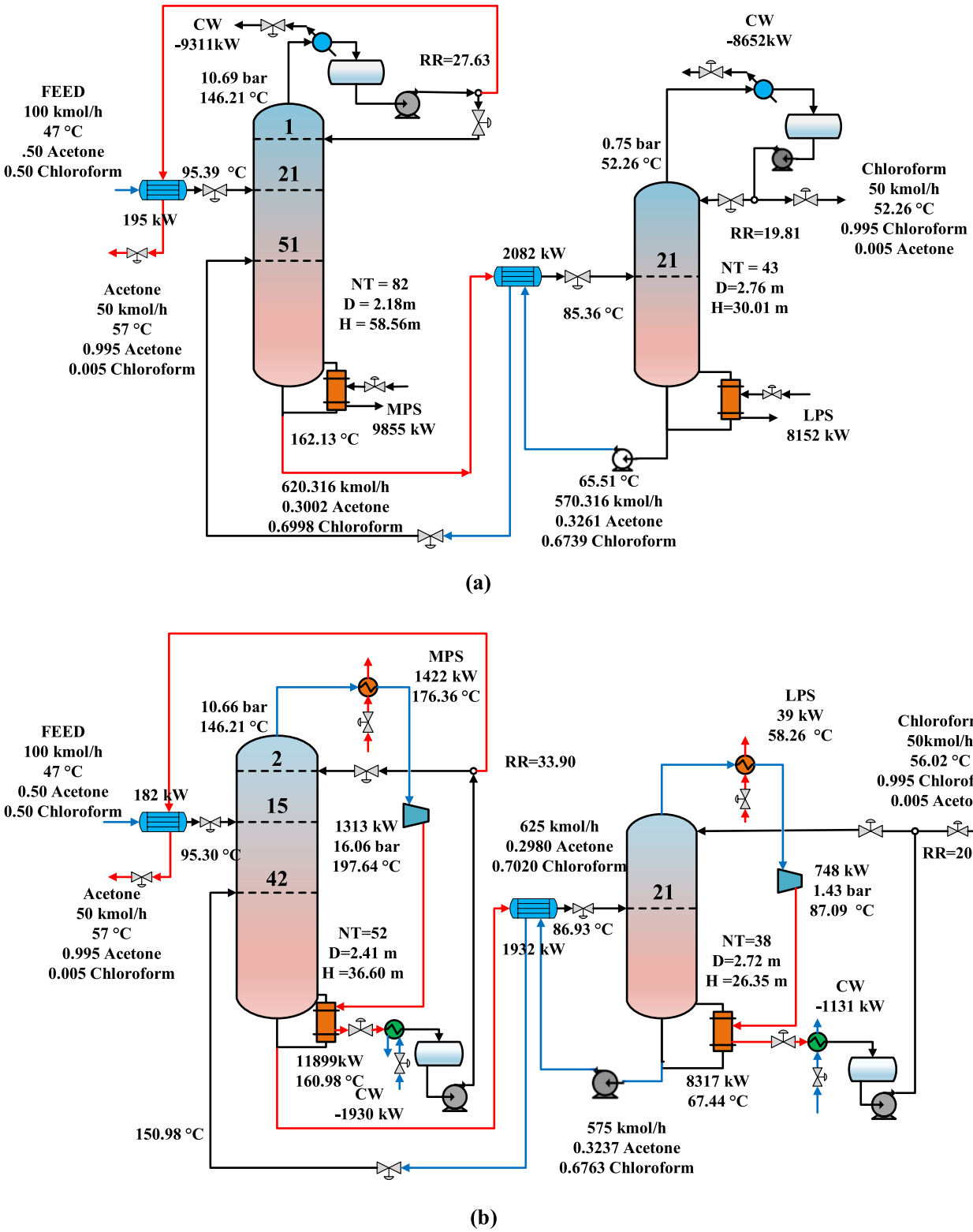

Fig. 1. Processes studied: (a) PSD-CONV, (b) PSD-HPAD, and (c) PSD-SHRT.

where, $b_j^{(1)}$ *and* $b_k^{(2)}$ are bias terms. As these terms are constants, their derivation is straightforward and thus omitted in the subsequent procedures to streamline the derivation process.

2.3. Evaluation measures

2.3.1. Predicted performance evaluation indexes

To assess the predictive performance of the neural network models, we utilize two key metrics: *MSE* and the coefficient of determination (R^2). *MSE* is a widely adopted criterion for quantifying the deviation

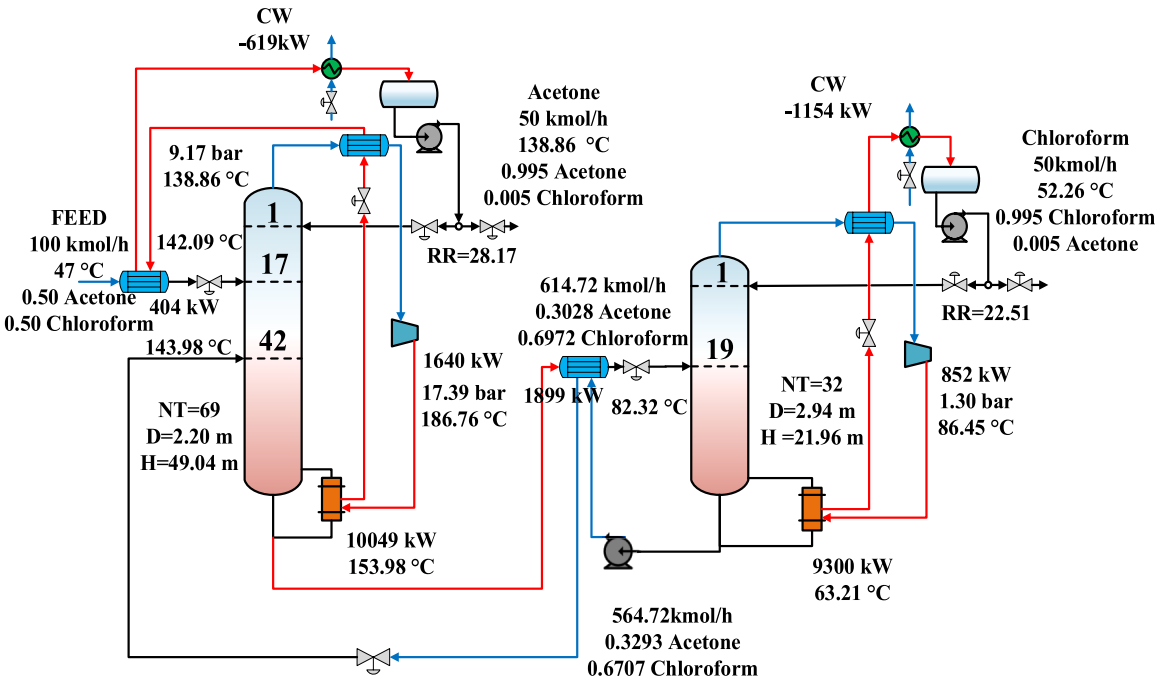

(c)

Fig. 1. (*continued*).

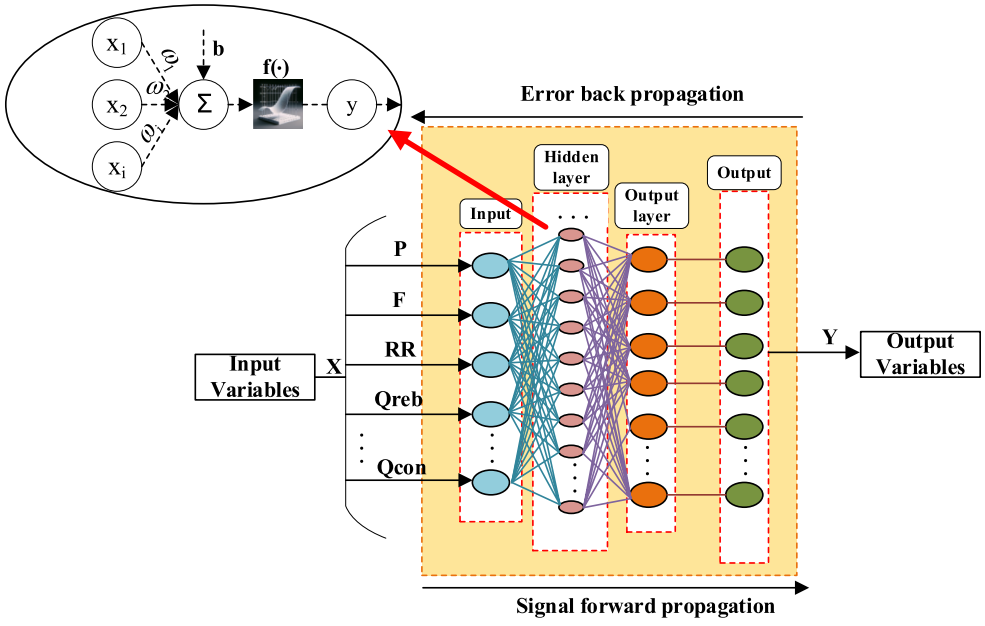

Fig. 2. The prediction principle based on ANN.

between predicted and observed values [37]. It is defined as the average of the squared differences between each pair of predicted and actual values, as described in Eq. (3):

$$MSE = \frac{1}{m}\sum_{k=1}^{m}(y_k - y_l)^2 \tag{3}$$

where y_k denotes the actual value, y_l represents the predicted value, and m is the sample size. The smaller the value of *MSE*, the higher the accuracy. Conversely, R^2 serves as an indicator of the correlation between the predicted outcomes and the actual target values [38], as described in Eq. (4):

$$R^2 = 1 - \frac{\sum_{t=1}^{n}(S_{ta} - S_{tp})}{\sum_{t=1}^{n}(S_{ta} - \overline{S_{tp}})} \tag{4}$$

S_{ta} represents the actual target values, S_{tp} denotes the predicted values generated by the model, $\overline{S_{tp}}$ is the mean of the actual observed values, n is the number of observations. An R^2 value approaching 1 signifies a higher level of performance efficiency and accuracy in the predictive

model.

2.3.2. Dynamic performance evaluation indexes

The integral of the squared error (ISE) measures the degree of excellence of dynamic control system performance when there is a disturbance in the process. It is a type of comprehensive indicator. The smaller the *ISE*, the better the performance of the dynamic control [39]. The *ISE* is defined as follows:

$$ISE = \int_{t_0}^{T} (y - y^{sp})^2 dt \tag{5}$$

where t_0 represents the initial time of the dynamic process. y and y^{sp} are the actual product purity the during disturbance process and the purity of the set product.

2.4. Principle of intelligent control

Recent studies on the distillation control [25,26,33,34,40,41] have highlighted a crucial conclusion: to ensure that product purity meets production requirements under varying feed conditions, temperature controllers must adjust to a new set point rather than maintaining the initial one. In conventional temperature control loops, the temperature set point (TSP) is either fixed or adjusted manually based on operator judgment. Conversely, in CC-TC systems, the TSP automatically adapts to changes in product purity, resulting in improved control performance. However, achieving the dynamic simulations accuracy in product composition measurements can pose practical challenges.

The dynamic optimization control model, as detailed in Fig. 3, comprises three primary components: the ANN modules, the Aspen Dynamic Modeler block, and the output signal display modules. The Neural NETwork model (NNET) is a trained neural network that has been integrated into the Simulink model for system simulation and analysis. Unlike traditional cascade control systems, which directly use product composition as the controlled variable, the intelligent control strategy employs an ANN to train on a comprehensive range of process variables to effectively manage disturbances. In this model, the ANN recalculates the temperature set points of temperature-sensitive stage in HPC and LPC (TSP1 and TSP2) dynamically, based on the dynamic simulation state of the system, adjusting these TSPs continuously in response to changes in feed conditions. This approach ensures that product quality is consistently maintained at the desired level.

The Aspen Dynamic Modeler block serves as bridge between Aspen Dynamics and Simulink, allowing the dynamic simulation data retrieval from the PSD dynamic model and facilitating immediate process adjustment. After 0.5 h of dynamic operation, disturbance signals are introduced into the process, and the resulting output data are recorded, such as the actual pressure of the HPC (P1), reflux ratio (RR), and brake horsepower (Bpower). To systematically explore the system's response to varying conditions, we initially modify the feed conditions, incrementing by 4 % each time (±4 %, ±8 %, ±12 %, etc.), after allowing the system to stabilize for one hour following each adjustment. This incremental approach helps us to observe how the system behaves as we push the limits of throughput and composition changes. The maximum extents of these adjustments are set at ± 20 % throughput and ± 10 % acetone composition, relative to their initial conditions. This range ensures that we cover a broad spectrum of operational scenarios that the system might encounter. To ensure accuracy and detail in our data collection, we sample the system's state every 0.01 h, providing a high-resolution view of the system's dynamic behavior. Ultimately, our dataset is derived from four distinct operational conditions, specifically targeting ± 20 % throughput and ± 10 % acetone composition disturbances. This comprehensive dataset allows us to train and validate our models effectively, ensuring that they are robust and adaptable to the real-world fluctuations in the PSD process. This feedback loop is crucial for predicting the optimal TSP, which is then applied to the PSD dynamic model within Aspen Dynamics, facilitating the process optimization and control. The simulation system operates within Simulink over a runtime of 30 h, allowing for extensive testing and validation of the control strategy. The process is outlined as follows:

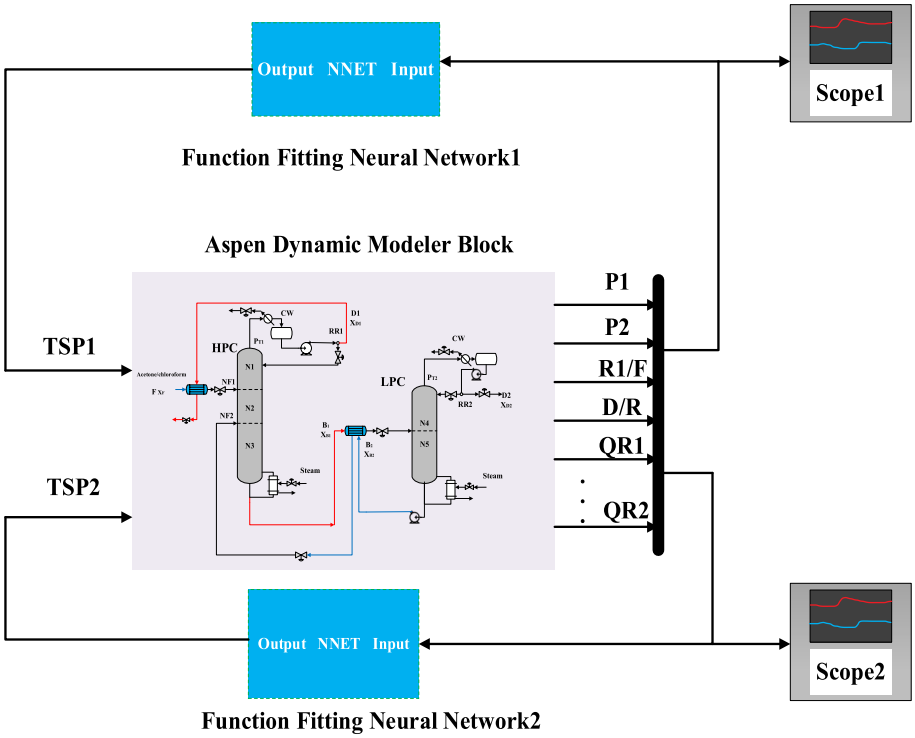

Fig. 3. Flowchart of the dynamic optimization control model based on ANNs.

1. **Data Acquisition**: Our previous work [25] demonstrated that single temperature control structures are effective in handling disturbances. However, to optimize TSPs, we require an extensive dataset that enables our model to determine the most appropriate TSPs effectively. Therefore, the training, validation, and testing datasets, which include all directly measurable process variables, are derived from the CC-TC system designed in this study. Essentially, the model simulates the behavior of the CC controller within this system, learning from the system's response to various disturbances.
2. **Variable Selection**: Incorporating too many process variables from the electrified PSD to predict the TSPs can lead to increased computational complexity. To enhance the efficiency of the prediction model, this study focuses on selecting process variables that exhibit a strong correlation with the TSPs, as determined through correlation analysis.
3. **ANN Model Development**: ANN model is trained, validated, and tested, with the objective of minimizing the error below a specified target threshold. Once the error meets this criterion, the trained ANN model—developed using the *gensim* function—is integrated into the PSD system via the AMsimulation module.
4. **System Testing**: The PSD process control system is evaluated by varying feed conditions within the Aspen Dynamics environment. The effectiveness of the intelligent control strategy is assessed by its ability to improve upon the single temperature control strategy and meet product specifications. If the control performance is found to be unsatisfactory, the process should return to step 1 for dataset regeneration and further refinement.

The intelligent control strategy for electrified PSD of acetone/chloroform azeotropes is designed to achieve precise product control while minimizing reliance on costly online composition detection instruments. Moreover, this approach can be extended to practical control structures in factories with varying degrees of automation, providing further validation of the feasibility of electrified distillation.

3. Dynamics and control

3.1. CC-TC control for PSD-CONV (CS1)

The PSD-CONV features independent reboilers and condensers, giving more control degrees of freedom and thus relatively easy to control. Our previous work [25] identified an effective temperature control structure (CS) that allowed product composition to return close to the set value under ± 20 % throughput variations and ± 10 % feed composition fluctuations. While this CS successfully mitigated disturbances, there remains potentials for further improvement in product purity. To address this, an enhanced control structure CS1 with CC-TC is developed, as demonstrated in Fig. 4(a). In this configuration, both $X_{D1,\ ACE}$ and $X_{D2,\ CHL}$ are controlled by manipulating the set points of the relevant cascaded temperature controllers. All other control loops and parameters remain consistent with the second CS developed for PSD-CONV in the previous work [25]. Table S1 shows the tuning parameters for the corresponding composition controllers.

After achieving stable operation of the closed-loop system for 0.5 h, disturbances of ± 20 % throughput and ± 10 % in acetone composition were introduced, with the test concluding at the 30 h. The effectiveness of control structure CS1 in managing these disturbances is shown in Fig. S2. The CS1 can maintain stable regulatory control with the CC-TC approach, restoring both product compositions to their original steady-state design specifications.

3.2. ANN-based dynamic control for PSD-CONV (CS2)

In this section, the ANN-based control strategy, which is built upon the CS1, is implemented. In the PI control strategy, variables such as flow rate, liquid level, pressure, reflux ratio, and temperature are more easily measurable compared to composition, and these readily measurable variables are listed in Table S2. Given the ease of obtaining these variables, they are selected as the input variables for the ANN. Inspired by the CC-TC control, there are two possible output variables for the ANN. One option is the product composition, where the ANN's output serves as the input for the PI composition controller. Alternatively, the ANN could output the set point of the temperature controller, thereby replacing the composition controller and functioning as the composition controller. The final output variable is selected based on its relevance to the input variables. In addition to selecting the output variables, the input variables must be selected carefully. Training, validating, and testing all potential variables involve additional computational effort, and including irrelevant input variables in the training process could negatively impact the accuracy of the predictions.

The selection of input and output variables is based on their correlation. The formula for calculating the correlation coefficient is as follows:

$$\rho_{X,Y} = \frac{E[(X - E(X))(Y - E(Y))]}{\sqrt{\sigma_X^2 \sigma_Y^2}} \tag{6}$$

where X and Y are variables, E represents mathematical expectation, σ^2 indicates variance, and ρ denotes the correlation coefficient. Retaining variables with high correlations and excluding those with low correlations is extremely meaningful for the training of neural networks [34]. Consequently, a threshold of 0.6 was established for correlation coefficient screening.

When the absolute value of the correlation coefficient between two variables is greater than or equal to 0.6, the correlation is considered as strong; otherwise, it is deemed weak. As shown in Fig. S3(a), the correlation between the variables and the product compositions ($X_{D1,ACE}$, $X_{D2,CHL}$) is generally weak. Only three basic variables (4, 9, 11) for $X_{D1,\ ACE}$ and two (9, 11) for $X_{D2,CHL}$ have absolute correlation coefficients greater than 0.6. However, when TSPs are used as output variables, two-thirds of the basic variables exhibit absolute correlation coefficients greater than 0.6, as depicted in Fig. S3(b). Therefore, TSPs are selected as the output variables for the ANN, and variables with correlation coefficients greater than 0.6 are chosen as the input variables. These final selected input variables have been bolded and underlined in Table S2 for clarity. The same approach has been applied to highlight the selected input variables in the subsequent PSD-HPAD and PSD-SHRT process variable tables. It can be observed that the selection of input variables remains the same regardless of whether TSP1 or TSP2 is chosen as the output. Consequently, the two ANN models can be effectively merged, which not only conserves computational resources but also enhances the accuracy and efficiency of the model.

In this section, we utilize a two-layer feed-forward network comprising hidden neurons with a Sigmoid activation function and output neurons with a linear activation function. The network structure, which consists of an input layer, a single hidden layer with 15 neurons, an output layer, and the final output, was determined through extensive training and testing to ensure optimal performance. The research data, generated from the anti-disturbance processes for ± 20 % throughput and ± 10 % acetone composition disturbances under PI control strategy, is divided into training data (70 %), validation data (15 %), and completely independent test data (15 %). The optimal ANN model is identified when the error is reduced to below the target threshold. To evaluate the performance of the developed model, we calculated the *MSE* and R^2 for the ANN. The *MSE* values being close to 0 and R^2 values being close to 1 demonstrate the accuracy of the ANNs. The *MSE* and R^2 for the training, validation, and test data are illustrated in Table. S3. Additionally, the error histogram shown in Fig. S4 visually displays the error between the predicted TSP and target TSP. The ordinate indicates the number of instances with corresponding errors. The errors are relatively small, mostly ranging between − 0.00206 and 0.00214, indicating that the predicted TSP closely matches the observed TSP. This

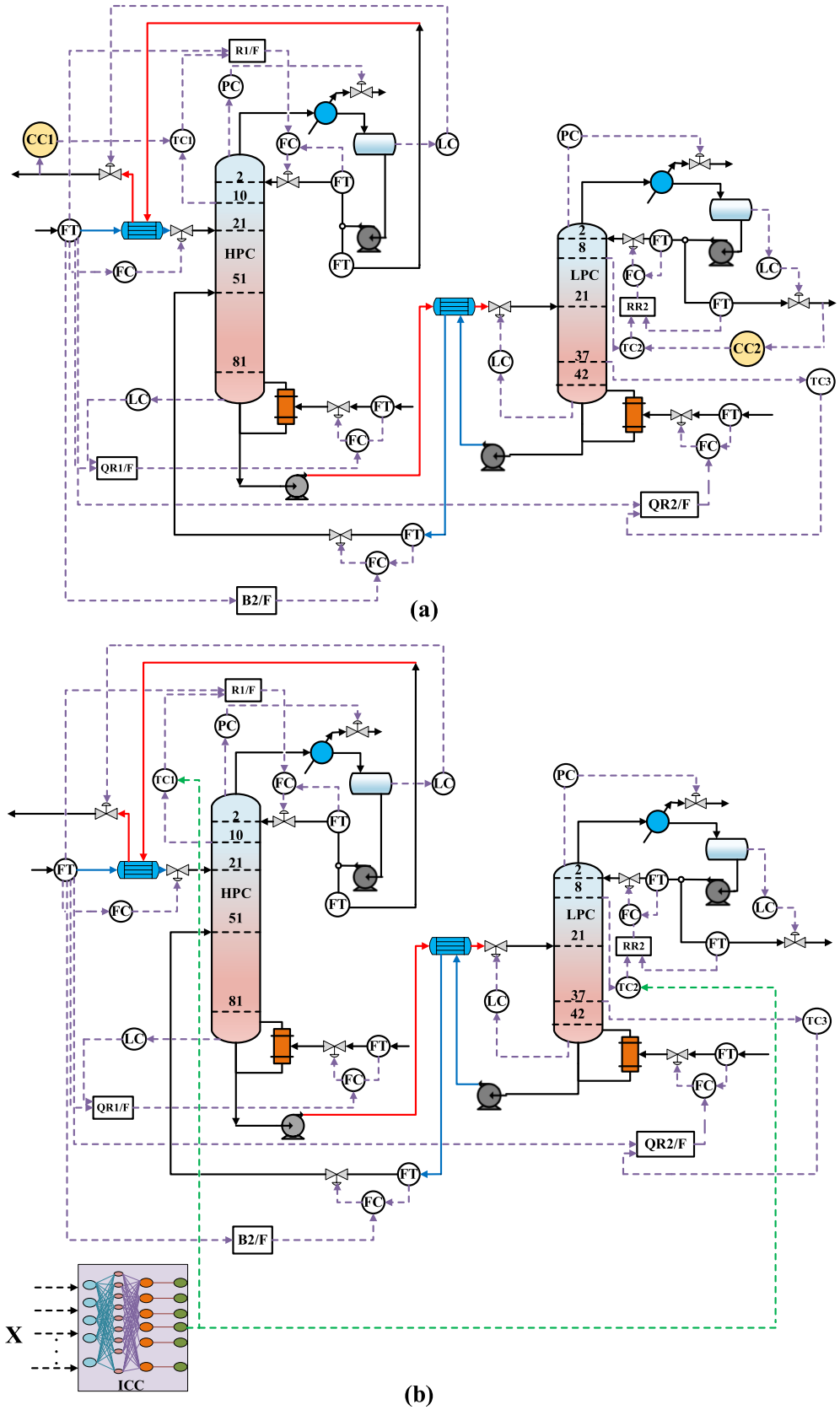

Fig. 4. CS for PSD-CONV: (a) CS1 with CC-TC, (b) CS2 with ICC-TC.

result confirms that the ANN structure is capable of accurately forecasting the output variables based on the input variables. It also validates the appropriateness of the selected variables and confirms the comprehensiveness of the dataset. These factors are crucial for designing an effective intelligent composition controller.

Fig. 4(b) illustrates the strategy for intelligent composition control (ICC) in the PSD-CONV process (CS2). The ICC-TC strategy shares the same objective as the CC-TC method, which is to automatically adjust the TSP to achieve precise control over the purity of the acetone/chloroform product. However, the underlying principles of the two methods are quite different. The ICC-TC uses easily measurable process variables as inputs, whereas the composition controller relies on composition values, which are challenging to measure online. The ICC-TC strategy considers two key perspectives. Economically, it eliminates the need for expensive component detection equipment. From a control standpoint, it effectively addresses the issue of delayed measurements.

In the CS1, ± 20 % throughput and ± 10 % acetone composition disturbances are applied to evaluate the performance, and the same disturbances are also test the CS2. Fig. 5 shows the anti-disturbance response curves under the ICC-TC. When comparing throughput disturbances to composition disturbances, the latter exhibits a smaller overshoot. Overall, the ICC-TC effectively bring the product composition back to the steady-state design specifications within a relatively short period of 15 h, highlighting their efficient performance.

3.3. CC-TC control for PSD-HPAD (CS3)

Building on our previous work [25], the control performance of the PSD-HPAD process has proven to be superior to that of the PSD-CONV process. Its dynamic controllability remains strong, despite the advantages of its steady-state design. However, similar to the dynamics and control outcomes of the PSD-CONV, there remains potential for further improvement in the product purities.

The control structure CS3 with CC-TC for PSD-HPAD is shown in Fig. 6(a). $X_{D1,ACE}$ and $X_{D2,CHL}$ are controlled by manipulating the set points of the associated cascaded temperature controllers. All other control loops and controller parameters remain identical to the third CS developed for PSD-HPAD in our previous work [25]. Table S4 gives the composition controller tuning parameters of CS3.

Fig. S5 presents the dynamic response results for large disturbances. The findings indicate that when dealing with disturbances of ± 20 % throughput and ± 10 mol% acetone composition, the compositions of the two distillates return to values closer to their steady-state design specifications. Compared to the dynamic performance of CS1, the range of product purity fluctuations for CS3 is more constrained, particularly when managing disturbances of ± 20 % throughput. Additionally, PSD-HPAD is a design that reduces costs and minimizes energy consumption. Therefore, improvements in the dynamic performance of product purity in PSD-HPAD are of significant importance.

3.4. ANN-based dynamic control for PSD-HPAD (CS4)

Table S5 and Fig. S6 present the process variables and the correlations among these variables for PSD-HPAD, respectively. As depicted in Fig. S6(a), the product compositions of HPC and LPC have correlation coefficients below 0.6 with other process variables, and $X_{D1,ACE}$ exhibits weak correlations with all process variables. In Fig. S6(b), it is evident that the TSPs of temperature-sensitive stages are generally have strong correlations with other process variables, although some differences exist. Notably, fewer process variables show strong correlations with TSP1 temperature-sensitive stage of the HPC. Consequently, it is more appropriate to use TSP as the output variable of the ANN. However, the selected process input variables differ, requiring the development of two separate ANN models for using TSP1 and the TSP2 as output variables. For PSD-HPAD, the same network structure used in PSD-CONV has been applied. Similarly, data from the resistance of the PI control strategy to feed disturbances were collected for training, validation, and testing the ANN model, with a sampling time of 0.01 h. The *MSE* and R^2 for training, validation, and testing are displayed in Table S6, and the close match between observed and predicted values in Fig. S7 confirms the accuracy of the ANN model's predictions. CS4 represents the intelligent composition control strategy for PSD-HPAD, and two ICCs have been designed as illustrated in Fig. 6(b).

Fig. 7 shows the disturbance resistance test results for CS4, where the fluctuations in product composition are minimal. All values stabilize within a very narrow range close to the set point after 15 h, demonstrating that the ICC-TC strategy meets production requirements.

3.5. CC-TC control for PSD-SHRT (CS5)

Unlike PSD-HPAD, the PSD-SHRT involves more heat exchangers and offers fewer control degrees of freedom [5]. As highlighted in our previous work [25], the control structure of PSD-SHRT integrates features from both PSD-CONV and PSD-HPAD, which have demonstrated promising stability. However, there is still potential for improving the purity of both acetone and chloroform products. In this section, CC-TC is proposed to further enhance $X_{D1,ACE}$ and $X_{D2,CHL}$. The CS5 with CC-TC for PSD-SHRT is shown in Fig. 8(a). All other control loops and controller parameters remain the same as those in the sixth CS developed for PSD-SHRT in previous work [25]. Table S7 provides the tuning parameters for the composition controllers in CS5.

Fig. S8 presents the dynamic response results for large disturbances. The results show that the compositions of the two distillates return to their steady-state design specifications when subjected to disturbances of ± 20 % throughput. Although the system did not fully return to its steady-state design specifications when dealing with disturbances of ± 10 % acetone composition, there has been a significant improvement compared to the previous single temperature control strategy.

3.6. ANN-based dynamic control for PSD-SHRT (CS6)

Table S8 and Fig. S9 present the process variables of PSD-SHRT and the correlation between these variables. Similar to the correlations observed in the PSD-HPAD process, as shown in Fig. S9(a), the product composition of HPC and LPC have correlation coefficients of less than 0.6 with other process variables, indicating relatively weak correlations. In Fig. S9(b), it is evident that the TSPs of temperature-sensitive stages generally have strong correlations with other process variables, although differences exist between them. Notably, fewer process variables show strong correlations with TSP1 in the HPC. As a result, it is more appropriate to use TSP as the output variable of the ANN, which is consistent with the variable correlation analysis seen in the PSD-HPAD process. However, since the selected process input variables differ for TSP1 and TSP2 as output variables, two separated ANN models must be established.

As discussed in CS4 regarding the ANN modeling effects, a lower number of variables does not necessarily lead to lower model accuracy; this can be adjusted by modifying the number of neurons and hidden layers. For PSD-SHRT, testing ultimately determined that the network structure should consist of an input layer, three hidden layers, an output layer, and the final output. The single hidden layer network specifically includes 25 neurons. Similarly, data on the resistance of the PI control strategy to feed disturbances were collected for training, validation, and testing of the ANN model, with a sampling time of 0.01 h. The *MSE* and R^2 values for training, validation, and testing are provided in Table S9, and the close match between observed and predicted values in Fig. S10 indicates the accuracy of the ANN model's predictions.

Fig. 8(b) shows ICC-TC strategy for PSD-SHRT (CS6). Fig. 9 shows the results of the anti-disturbance tests of intelligent control. The fluctuations in product composition are small, and they can all stabilize within a small range near the set value after 10 h, indicating that the ICC-TC strategy can meet production requirements.

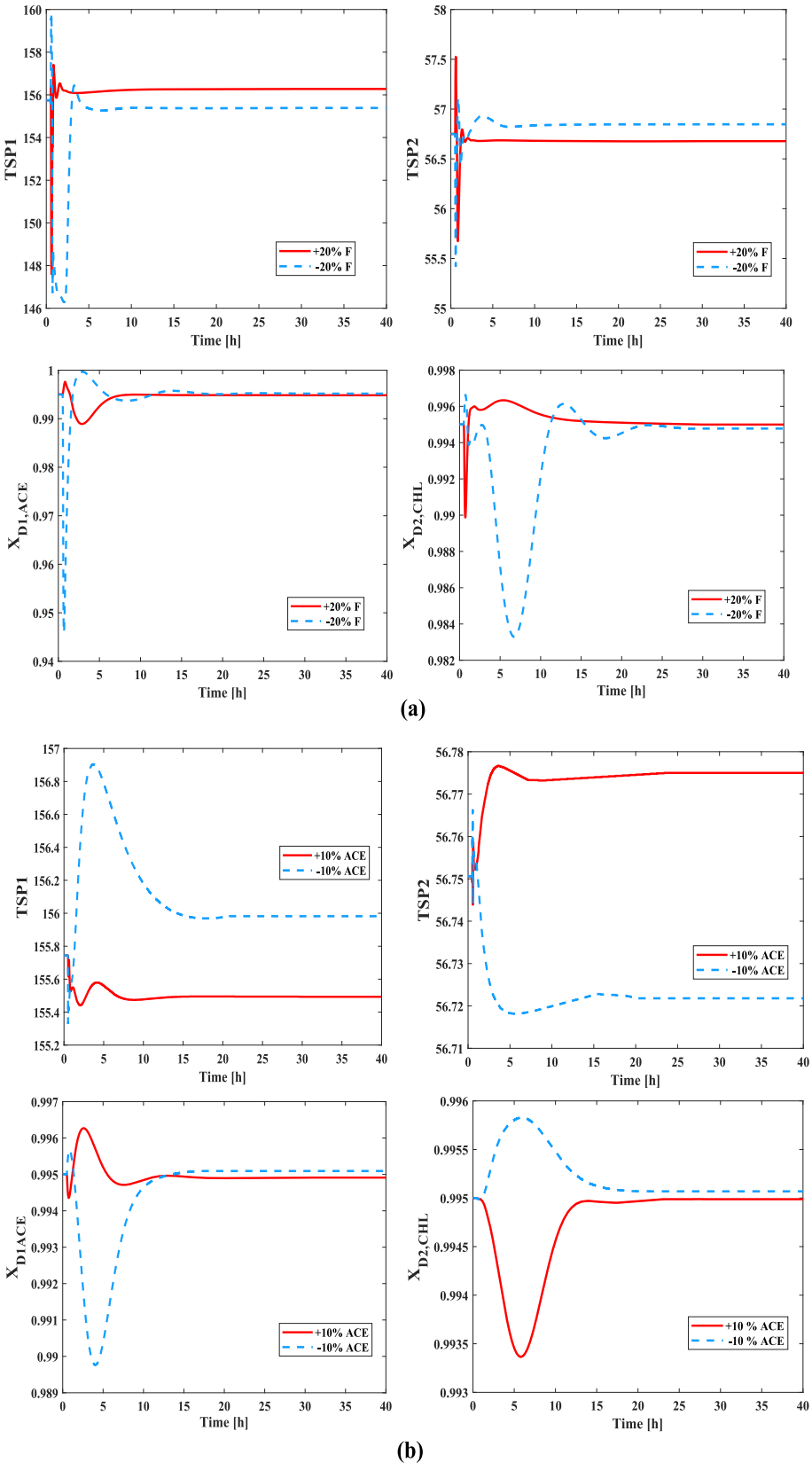

Fig. 5. Anti-disturbance results for CS2 with ICCs:(a) ± 20 % throughput and (b) ± 10 mol% acetone composition.

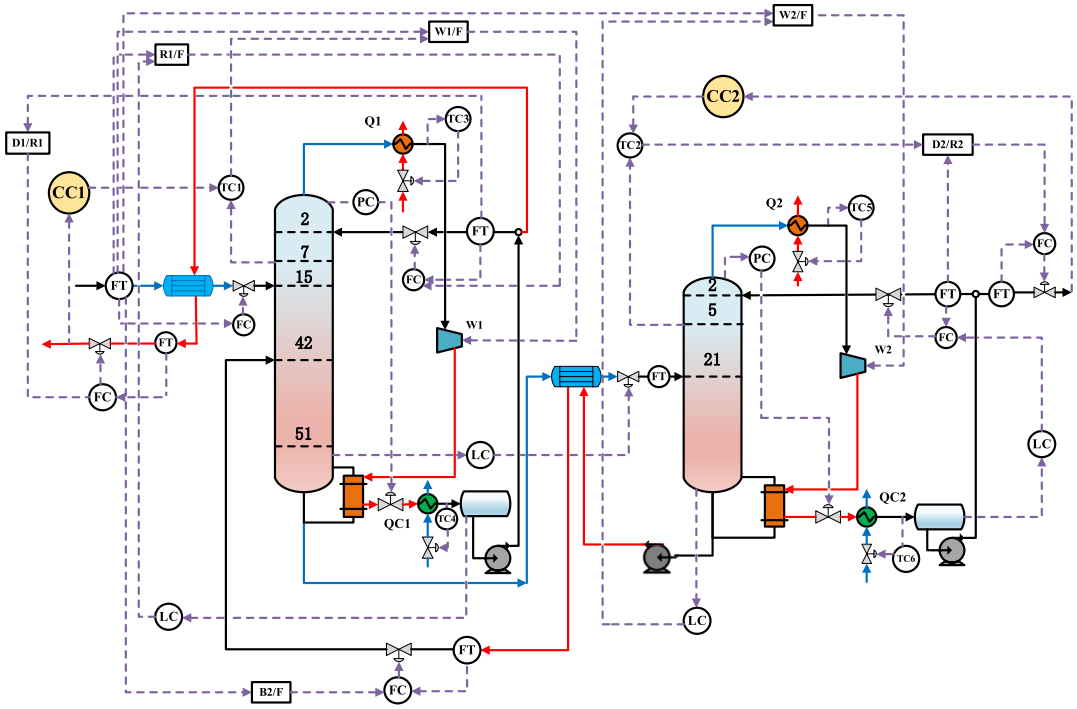

(a)

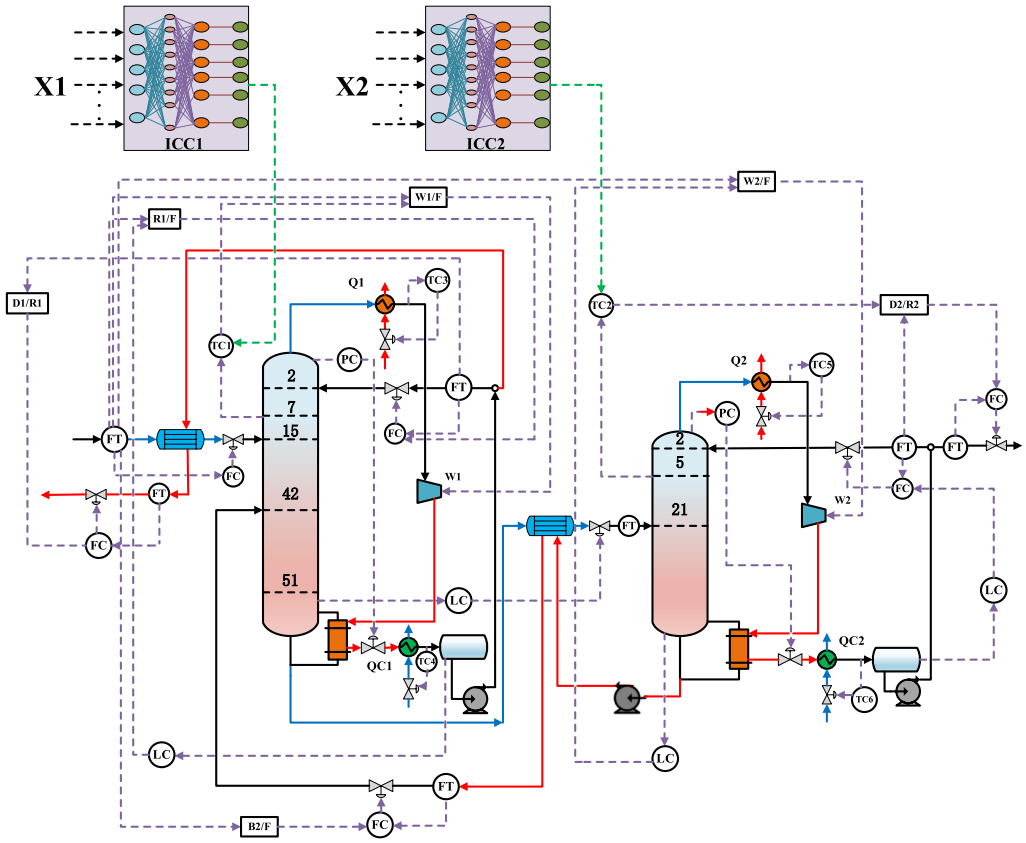

(b)

Fig. 6. CS for PSD-HPAD: (a) CS3 with CC-TC, (b) CS4 with ICC-TC.

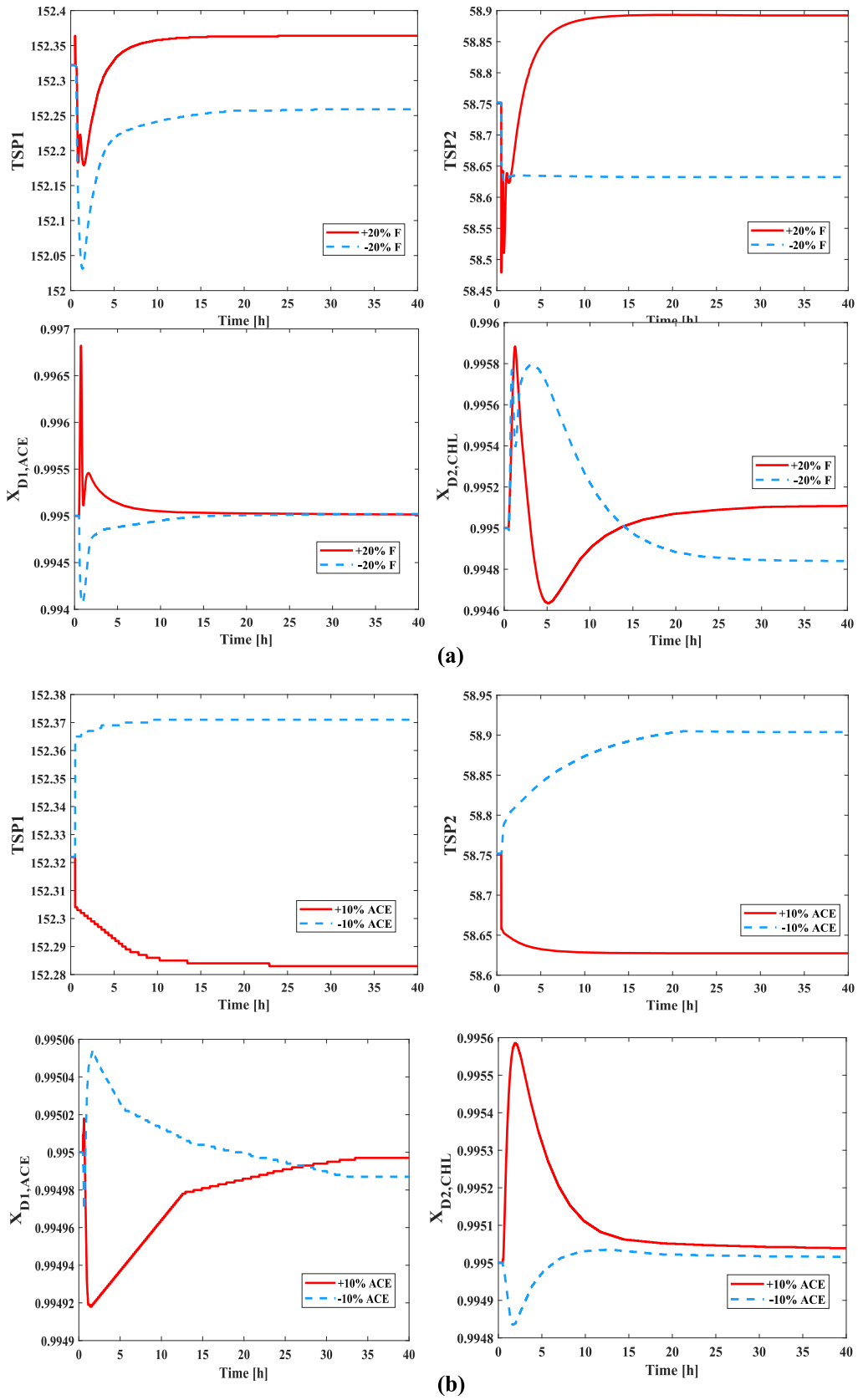

Fig. 7. Anti-disturbance results for CS4 with ICCs:(a) ± 20 % throughput and (b) ± 10 mol% acetone composition.

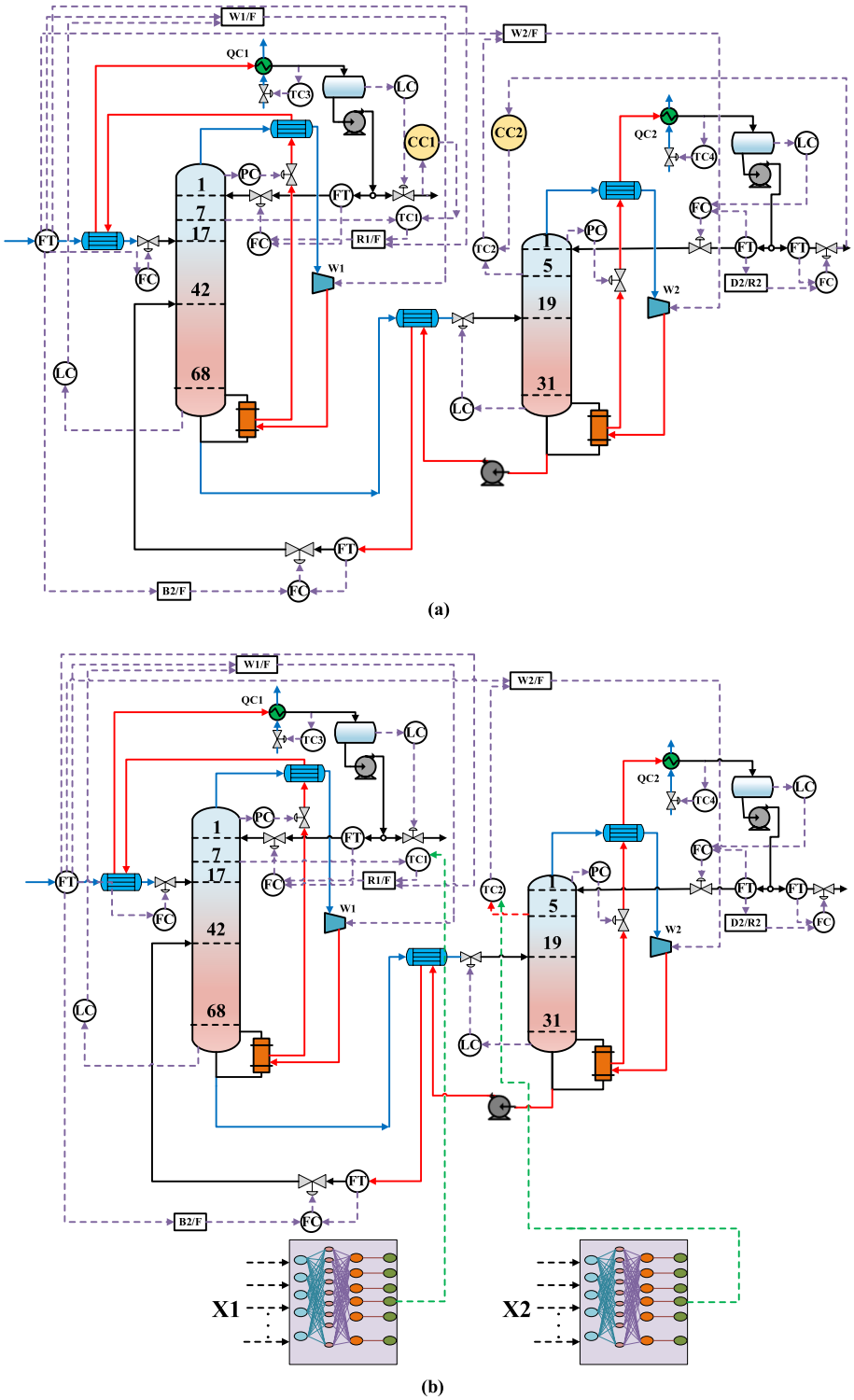

Fig. 8. CS for PSD-SHRT: (a) CS5 with CC-TC, (b) CS6 with ICC-TC.

4. Control performance comparisons

In this section, a comprehensive dynamic comparison of control structures is conducted to evaluate the performance of ICCs, encompassing CS1 and CS2 for PSD-CONV, CS3 and CS4 for PSD-HPAD, and CS5 and CS6 for PSD-SHRT. As depicted in Fig. 10, under ± 20 % throughput disturbances, the dynamic responses of CC-TC and ICC-TC for PSD-HPAD and PSD-SHRT are similar, with an anticipated transient time of 5 h for the controlled variables. In contrast, PSD-CONV exhibits a relatively longer transient time of approximately 15 h compared to PSD-HPAD and PSD-SHRT. Nevertheless, for ± 10 % acetone composition disturbances, the overshoot of the systems is minimal, and all products eventually stabilized within approximately 15 h. Furthermore, the dynamic response of ICCs for PSD-CONV is not superior to that of PSD-HPAD and PSD-SHRT. Regarding oscillation amplitude, PSD-CONV even show a higher amplitude than PSD-HPAD and PSD-SHRT.

The ISE values of the CSs have been meticulously calculated, and a

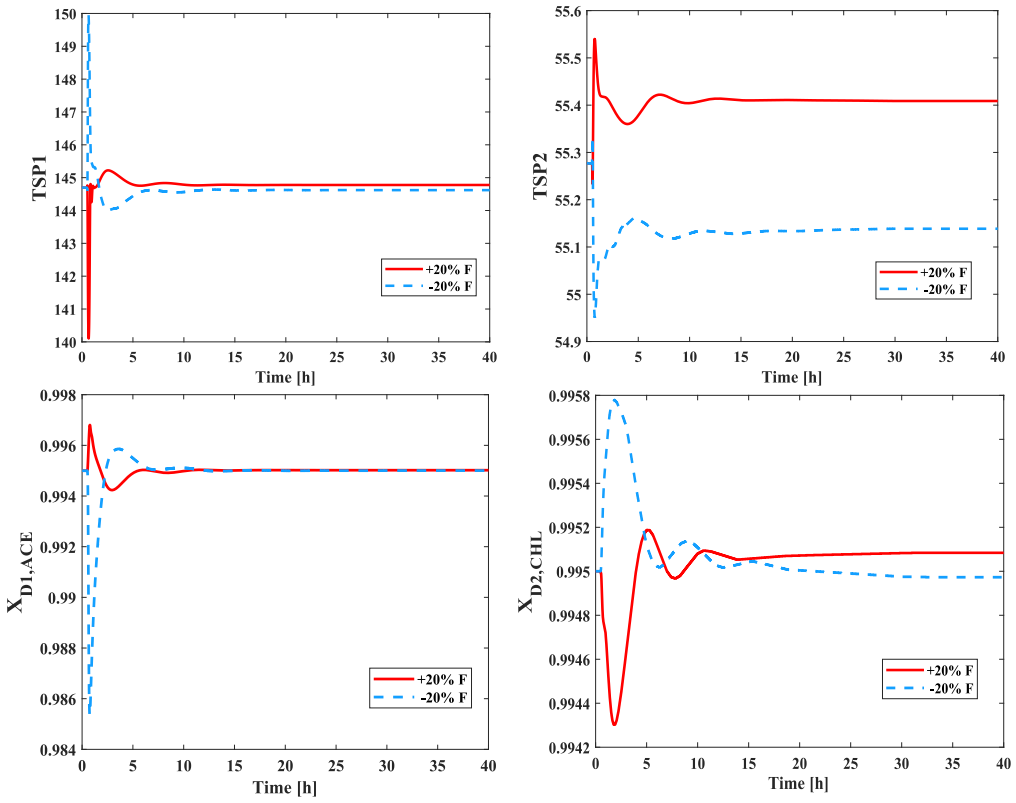

(a)

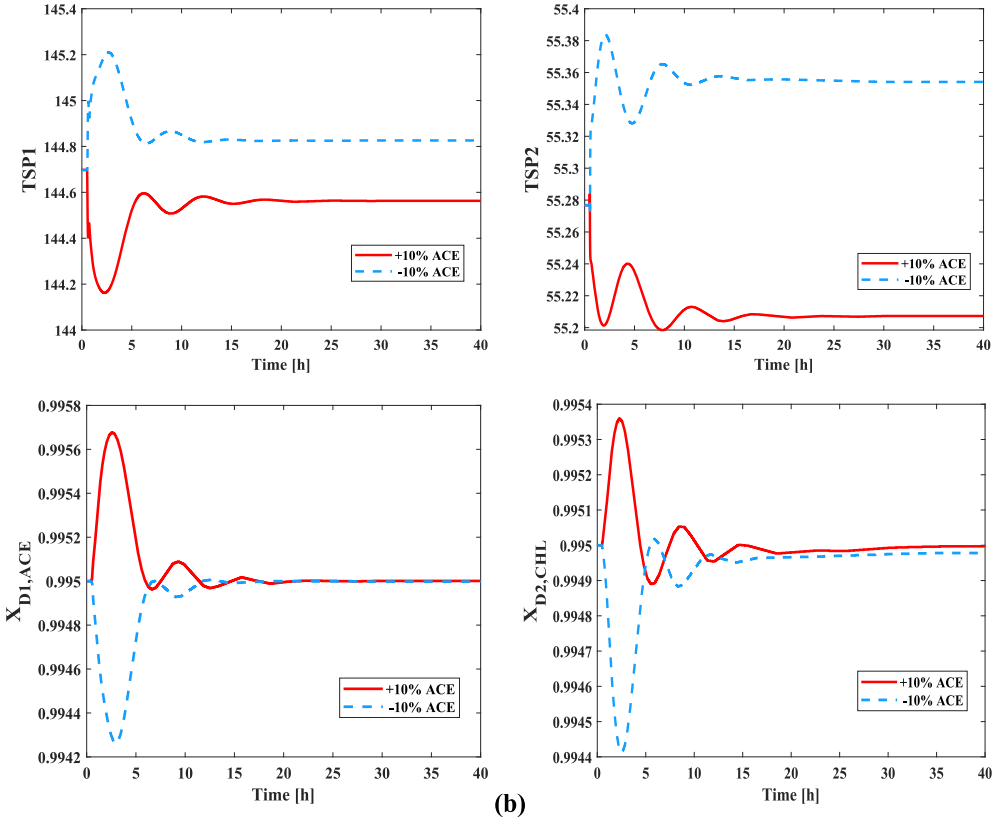

(b)

Fig. 9. Anti-disturbance results for CS6 with ICCs:(a) ± 20 % throughput and (b) ± 10 mol% acetone composition.

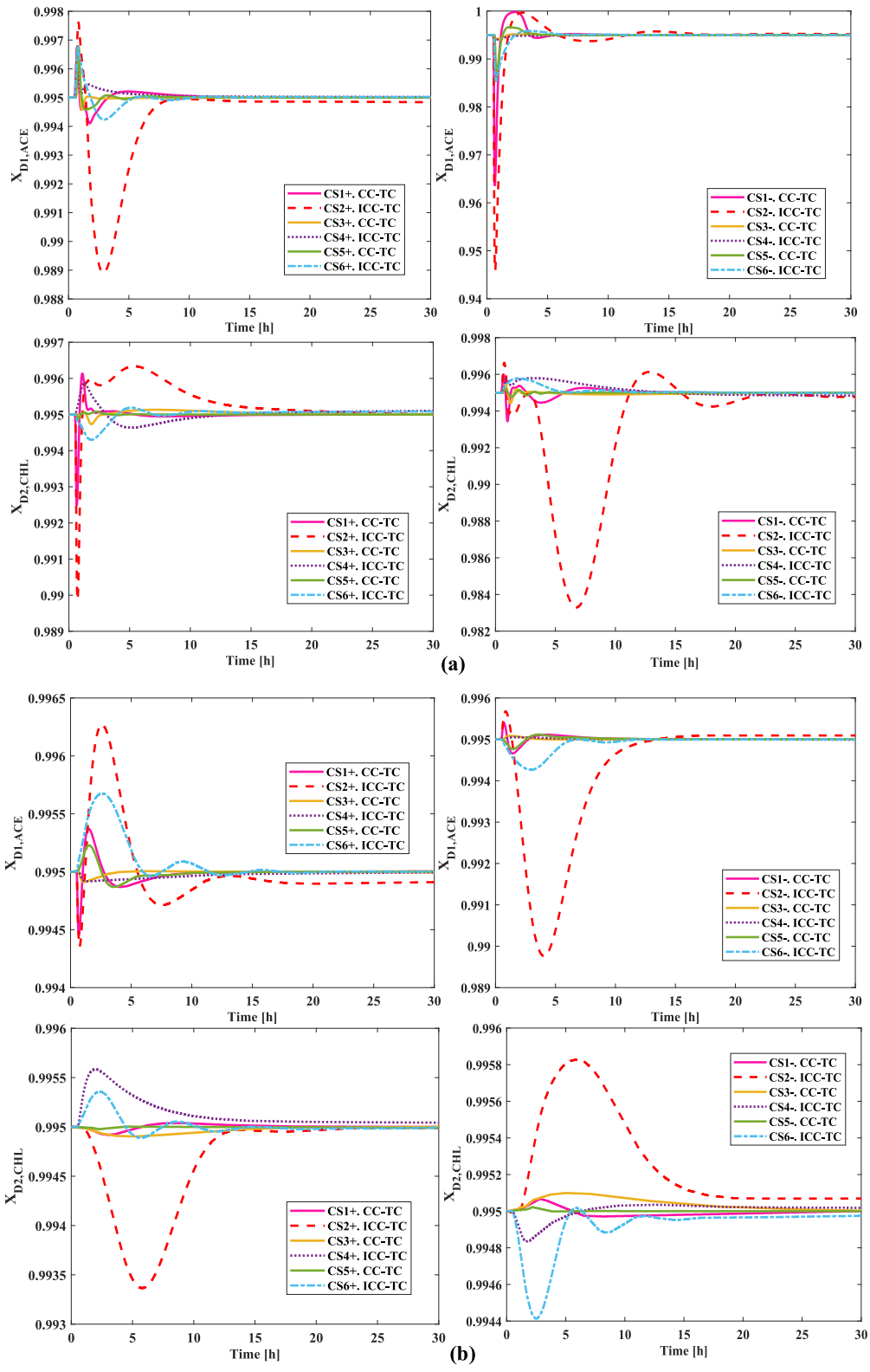

Fig. 10. Dynamic response performance comparisons of control structures for ± 20 % feed flowrate (a) and ± 10 % acetone composition (b) disturbances.

thorough analysis of the final steady-state results has been compiled. To provide a comprehensive assessment of their performance, we have compared these results with those obtained from the traditional single PI temperature control strategy. As shown in Tables 1 and 2, the performance of ICC-TC and CC-TC is very similar, maintaining comparable results for PSD-HPAD and PSD-SHRT. Notably, ICC-TC significantly outperformed the single temperature control strategy, indicating a substantial improvement in system robustness with minimal cost implications. Although the dynamic performance of ICC-TC in PSD-CONV is slightly weaker compared to CC-TC and the traditional TC strategy in terms of ISE, the overall dynamic performance of electrified distillation is generally good, making it a viable choice for industrial applications.

Table 1
ISE values for the different control structures.

Control structure	+20 % F	−20 % F	+10 % acetone	−10 % acetone
CS (TC) CONV				
ISE_{ACE}	4.8186e-05	0.00049918	9.1103e-05	3.6902e-05
ISE_{CHL}	1.3703e-05	5.0845e-05	6.4588e-05	6.985e-06
CS1(CC-TC)				
ISE_{ACE}	1.2416e-06	0.00022037	2.1431e-07	1.6066e-07
ISE_{CHL}	1.3869e-06	1.3509e-06	2.0497e-08	1.4931e-08
CS2(ICC-TC)				
ISE_{ACE}	8.3097e-05	0.00084526	3.6371e-06	8.7034e-05
ISE_{CHL}	1.5911e-05	6.0477e-05	8.1264e-06	4.3056e-06
CS(TC) HPAD				
ISE_{ACE}	1.3609e-06	1.4734e-06	2.5445e-07	2.6556e-07
ISE_{CHL}	1.87e-05	1.9897e-05	1.6709e-05	1.8994e-05
CS3(CC-TC)				
ISE_{ACE}	5.2826e-07	4.0584e-07	9.2617e-09	9.1666e-09
ISE_{CHL}	1.5371e-07	2.1067e-07	6.2781e-08	8.2649e-08
CS4(ICC-TC)				
ISE_{ACE}	9.3371e-07	7.5666e-07	4.0537e-08	9.5596e-09
ISE_{CHL}	7.2315e-07	8.6027e-07	8.206e-07	6.3232e-08
CS(TC) SHRT				
ISE_{ACE}	2.4135e-06	4.1229e-05	9.8493e-06	7.0683e-06
ISE_{CHL}	2.0188e-05	2.7628e-05	2.8931e-05	2.023e-05
CS5(CC-TC)				
ISE_{ACE}	6.7809e-07	2.019e-05	7.6591e-08	7.3455e-08
ISE_{CHL}	7.5666e-09	3.8639e-08	1.2029e-09	4.3548e-10
CS6(ICC-TC)				
ISE_{ACE}	8.0728e-07	3.2406e-05	7.1602e-07	8.3825e-07
ISE_{CHL}	8.8105e-08	8.4868e-07	9.618e-08	7.4955e-08

Table 2
Comparison of closed-loop responses in product compositions.

Control structure	Target	+20 % F	−20 % F	+10 % acetone	−10 % acetone
CS (TC) CONV					
$X_{D1,ACE}$	0.995000	0.995929	0.994175	0.993194	0.995451
$X_{D2,CHL}$	0.995000	0.994295	0.995719	0.996046	0.994518
CS1 (CC-TC)					
$X_{D1,ACE}$	0.995000	0.994997	0.994999	0.995003	0.994999
$X_{D2,CHL}$	0.995000	0.995001	0.995000	0.995000	0.995000
CS2 (ICC-TC)					
$X_{D1,ACE}$	0.995000	0.994838	0.995167	0.994911	0.995094
$X_{D2,CHL}$	0.995000	0.994997	0.994777	0.994988	0.995069
CS (TC) HPAD					
$X_{D1,ACE}$	0.995000	0.995126	0.995960	0.994915	0.994140
$X_{D2,CHL}$	0.995000	0.994888	0.993942	0.995084	0.996000
CS3(CC-TC)					
$X_{D1,ACE}$	0.995000	0.995004	0.994991	0.995000	0.995000
$X_{D2,CHL}$	0.995000	0.995000	0.994998	0.995000	0.995004
CS4(ICC-TC)					
$X_{D1,ACE}$	0.995000	0.995017	0.995015	0.994994	0.994990
$X_{D2,CHL}$	0.995000	0.995073	0.994855	0.995030	0.995018
CS (TC) SHRT					
$X_{D1,ACE}$	0.995000	0.995169	0.995852	0.994434	0.993969
$X_{D2,CHL}$	0.995000	0.994842	0.993996	0.995428	0.995871
CS5(CC-TC)					
$X_{D1,ACE}$	0.995000	0.995000	0.995000	0.995003	0.995000
$X_{D2,CHL}$	0.995000	0.995000	0.995000	0.994990	0.995000
CS6(ICC-TC)					
$X_{D1,ACE}$	0.995000	0.995019	0.995004	0.995001	0.994998
$X_{D2,CHL}$	0.995000	0.995051	0.994976	0.994993	0.994975

Overall, ICCs effectively return product composition to the set values within a short period. Despite slightly larger system fluctuations under intelligent control compared to CC-TC control, the key advantage is the elimination of the need for online product composition measurement. Furthermore, under intelligent composition control strategies, the controllability of electrified distillation—offering enhanced energy efficiency—generally surpassed that of traditional methods, emphasizing its suitability for industrial applications.

5. Conclusions

This work presents a novel approach to control the electrified PSD of a maximum-boiling acetone/chloroform azeotrope, focusing on the development of an ICC based on ANNs. While prior studies have investigated the separation of this azeotrope, our research distinguishes itself by introducing an innovative control structure that effectively eliminates the need for online composition measurements, a significant limitation in existing methods. The ANN model is developed using easily measurable process variables identified through correlation analysis, enhancing practicality in real-world applications. We successfully integrated the ICC with traditional PID controllers to form a cascade control structure, referred to as ICC-TC. A notable advantage of this structure is its flexibility feature, allowing the system to continue operating reliably with a PI temperature controller in the event of ICC failure. Furthermore, under conditions of substantial throughput and composition disturbances, ICC-TC demonstrated the capability to maintain product purity levels comparable to those achieved by conventional cascade control methods. This research underscores the potential of electrified distillation in promoting economic and environmental sustainability. Future studies will aim to leverage advanced neural networks and sophisticated control algorithms to further enhance control performance and efficiency in electrified PSD applications, highlighting the significance of our contributions to the field.

Declaration of competing interest

The authors declare that they have no known competing financial interests or personal relationships that could have appeared to influence the work reported in this paper.

Acknowledgments

This work was supported by the National Natural Science Foundation of China (Grant No. 22208154) and Natural Science Foundation of Jiangsu Province (Grant No. BK20220348).

Appendix A. Supplementary data

Supplementary data to this article can be found online at https://doi.org/10.1016/j.seppur.2024.130991.

References

[1] C. Cui, M. Qi, X. Zhang, J. Sun, Q. Li, A.A. Kiss, M. Lee, Electrification of distillation for decarbonization: An overview and perspective, Renew. Sustain. Energy Rev. 199 (2024) 114522, https://doi.org/10.1016/j.rser.2024.114522.

[2] J. Rockström, O. Gaffney, J. Rogelj, M. Meinshausen, N. Nakicenovic, H. J. Schellnhuber, A roadmap for rapid decarbonization, Science 355 (6331) (2017) 1269–1271, https://doi.org/10.1126/science.aah3443.

[3] E. Papadis, G. Tsatsaronis, Challenges in the decarbonization of the energy sector, Energy 205 (2020) 118025, https://doi.org/10.1016/j.energy.2020.118025.

[4] W.L. Luyben, Importance of pressure-selection in pressure-swing distillation, Comput. Chem. Eng. 149 (2021) 107279, https://doi.org/10.1016/j.compchemeng.2021.107279.

[5] C. Cui, N.V.D. Long, J. Sun, M. Lee, Electrical-driven self-heat recuperative pressure-swing azeotropic distillation to minimize process cost and CO2 emission: Process electrification and simultaneous optimization, Energy 195 (2020) 116998, https://doi.org/10.1016/j.energy.2020.116998.

[6] X. Liu, Q. Xu, C. Ma, F. Zhang, P. Cui, Y. Wang, B. Shan, Design and multi-objective optimization of reactive pressure-swing distillation process for separating tetrahydrofuran-methanol-water, Sep. Purif. Technol. 329 (2024) 125160, https://doi.org/10.1016/j.seppur.2023.125160.

[7] Z. Lei, C. Li, B. Chen, Extractive distillation: a review, Sep. Purif. Rev. 32 (2) (2003) 121–213, https://doi.org/10.1081/SPM-120026627.

[8] J. Huang, Q. Zhang, C. Liu, T. Yin, W. Xiang, Optimal design of the ternary azeotrope separation process assisted by reactive-extractive distillation for ethyl acetate/isopropanol/water, Sep. Purif. Technol. 306 (2023) 122708, https://doi.org/10.1016/j.seppur.2022.122708.

[9] X. Zhang, C. Cui, J. Sun, X. Zhang, Integrated design and self-optimizing control of extractive distillation process with preconcentration, Chem. Eng. Sci. 280 (2023) 119074, https://doi.org/10.1016/j.ces.2023.119074.

[10] X. Li, Q. Ye, J. Li, Y. Liu, L. Yan, X. Jian, J. Zhang, Investigation on energy-efficient heterogeneous pressure-swing azeotropic distillation for recovery of cyclohexane and tert-butanol from industrial effluent, Sep. Purif. Technol. 306 (2023) 122705, https://doi.org/10.1016/j.seppur.2022.122705.

[11] Y. Ma, Z. Hu, X. Sun, Z. Shen, X. Li, J. Gao, Y. Wang, Energy-saving design of azeotropic distillation for the separation of methanol–methyl methacrylate azeotrope from industrial effluent, Sep. Purif. Technol. 353 (2025) 128382, https://doi.org/10.1016/j.seppur.2024.128382.

[12] W.L. Luyben, I.L. Chien, in: Design and control of distillation systems for separating azeotropes, John Wiley & Sons, 2011, https://doi.org/10.1002/9780470575802.

[13] Y. Wang, Z. Zhang, D. Xu, W. Liu, Z. Zhu, Design and control of pressure-swing distillation for azeotropes with different types of boiling behavior at different pressures, J. Process Control 42 (2016) 59–76, https://doi.org/10.1016/j.jprocont.2016.04.006.

[14] Z. Zhu, L. Wang, Y. Ma, W. Wang, Y. Wang, Separating an azeotropic mixture of toluene and ethanol via heat integration pressure swing distillation, Comput. Chem. Eng. 76 (2015) 137–149, https://doi.org/10.1016/j.compchemeng.2015.02.016.

[15] Z. Zhu, D. Xu, H. Jia, Y. Zhao, Y. Wang, Heat integration and control of a triple-column pressure-swing distillation process, Ind. Eng. Chem. Res. 56 (8) (2017) 2150–2167, https://doi.org/10.1021/acs.iecr.6b04118.

[16] F. Zhang, D. Sun, Y. Li, B. Shan, Y. Ma, Y. Wang, Z. Zhu, Heat integration and dynamic control for separating the ternary azeotrope of butanone/isopropanol/n-heptane via pressure-swing distillation, Chem. Eng. Process.-Process Intensification 170 (2022) 108657, https://doi.org/10.1016/j.cep.2021.108657.

[17] Q. Zhang, M. Liu, C. Li, A. Zeng, Heat-integrated pressure-swing distillation process for separation of the maximum-boiling azeotrope diethylamine and methanol, J. Taiwan Inst. Chem. Eng. 93 (2018) 644–659, https://doi.org/10.1016/j.jtice.2018.09.018.

[18] X. Li, X. Geng, P. Cui, J. Yang, Z. Zhu, Y. Wang, D. Xu, Thermodynamic efficiency enhancement of pressure-swing distillation process via heat integration and heat pump technology, Appl. Therm. Eng. 154 (2019) 519–529, https://doi.org/10.1016/j.applthermaleng.2019.03.118.

[19] N. Wang, Q. Ye, L. Chen, H. Zhang, J. Zhong, Improving the economy and energy efficiency of separating water/acetonitrile/isopropanol mixture via triple-column pressure-swing distillation with heat-pump technology, Energy 215 (2021) 119126, https://doi.org/10.1016/j.energy.2020.119126.

[20] J. Zhai, X. Chen, X. Sun, H. Xie, Economically and thermodynamically efficient pressure-swing distillation with heat integration and heat pump techniques, Appl. Therm. Eng. 218 (2023) 119389, https://doi.org/10.1016/j.applthermaleng.2022.119389.

[21] N.M. Nikačević, A.E. Huesman, P.M. Van den Hof, A.I. Stankiewicz, Opportunities and challenges for process control in process intensification, Chem. Eng. Process. 52 (2012) 1–15, https://doi.org/10.1016/j.cep.2011.11.006.

[22] I. Patraşcu, C.S. Bildea, A.A. Kiss, Dynamics and control of a heat pump assisted extractive dividing-wall column for bioethanol dehydration, Chem. Eng. Res. Des. 119 (2017) 66–74, https://doi.org/10.1016/j.cherd.2016.12.021.

[23] D. Sun, Q. Xu, F. Zhang, Z. Zhu, Y. Wang, P. Cui, B. Shan, Product composition control based on backpropagation neural network in pressure-swing distillation processes, Chem. Eng. Process.-Process Intensification 183 (2023) 109224, https://doi.org/10.1016/j.cep.2022.109224.

[24] S. Liang, Y. Cao, X. Liu, X. Li, Y. Zhao, Y. Wang, Y. Wang, Insight into pressure-swing distillation from azeotropic phenomenon to dynamic control, Chem. Eng. Res. Des. 117 (2017) 318–335, https://doi.org/10.1016/j.cherd.2016.10.040.

[25] D. Yang, Q. Zhang, Q. Zhang, C. Cui, Dynamics and control of electrified pressure-swing distillation for separating a maximum-boiling azeotrope featuring small pressure-induced shift, Sep. Purif. Technol. 312 (2023) 123360, https://doi.org/10.1016/j.seppur.2023.123360.

[26] C. Cui, Q. Zhang, X. Zhang, J. Sun, I.L. Chien, Dynamics and control of thermal-versus electrical-driven pressure-swing distillation to separate a minimum-boiling azeotrope, Sep. Purif. Technol. 280 (2022) 119839, https://doi.org/10.1016/j.seppur.2021.119839.

[27] A. Chari, S. Christodoulou, Building energy performance prediction using neural networks, Energ. Effi. 10 (5) (2017) 1315–1327, https://doi.org/10.1007/s12053-017-9524-5.

[28] C. Johnstone, E.D. Sulungu, Application of neural network in prediction of temperature: a review, Neural Comput. Applic. 33 (18) (2021) 11487–11498, https://doi.org/10.1007/s00521-020-05582-3.

[29] Y. Wang, Z. Han, Y. Xing, S. Xu, J. Wang, A survey on datasets for the decision making of autonomous vehicles, IEEE Intell. Transp. Syst. Mag. (2024), https://doi.org/10.1109/MITS.2023.3341952.

[30] J.R. Van Leeuwen, E.L. Penne, T. Rabelink, R. Knevel, Y.O. Teng, Using an artificial intelligence tool incorporating natural language processing to identify patients with a diagnosis of ANCA-associated vasculitis in electronic health records, Comput. Biol. Med. 168 (2024) 107757, https://doi.org/10.1016/j.compbiomed.2023.107757.

[31] W. Hu, X. Li, C. Li, R. Li, T. Jiang, H. Sun, X. Li, A state-of-the-art survey of artificial neural networks for whole-slide image analysis: from popular convolutional neural networks to potential visual transformers, Comput. Biol. Med. 161 (2023) 107034, https://doi.org/10.1016/j.compbiomed.2023.107034.

[32] G. Kataria, K. Singh, Recurrent neural network based soft sensor for monitoring and controlling a reactive distillation column, Chem. Prod. Process Model. 13 (3) (2018) 20170044, https://doi.org/10.1515/cppm-2017-0044.

[33] B. Shan, C. Ma, C. Niu, Q. Xu, Z. Zhu, Y. Wang, F. Zhang, Soft sensor model predictive control for azeotropic distillation of the separation of DIPE/IPA/water mixture, J. Taiwan Inst. Chem. Eng. 152 (2023) 105185, https://doi.org/10.1016/j.jtice.2023.105185.

[34] H. Li, W. Wang, Y. Wang, C. Li, Y. Wang, Z. Zhu, Y. Li, Dynamic real-time energy saving control of pressure-swing distillation based on artificial neural networks, Chem. Eng. Sci. 282 (2023) 119271, https://doi.org/10.1016/j.ces.2023.119271.

[35] W.L. Luyben, Comparison of extractive distillation and pressure-swing distillation for acetone/chloroform separation, Comput. Chem. Eng. 50 (2013) 1–7, https://doi.org/10.1016/j.compchemeng.2012.10.014.

[36] F. Yu, X. Xu, A short-term load forecasting model of natural gas based on optimized genetic algorithm and improved BP neural network, Appl. Energy 134 (2014) 102–113, https://doi.org/10.1016/j.apenergy.2014.07.104.

[37] O. Köksoy, Multiresponse robust design: Mean square error (MSE) criterion, Appl. Math Comput. 175 (2) (2006) 1716–1729, https://doi.org/10.1016/j.amc.2005.09.016.

[38] H. Song, M. Kim, D. Park, Y. Shin, J.G. Lee, Learning from noisy labels with deep neural networks: A survey, IEEE Trans. Neural Networks Learn. Syst. 34 (11) (2022) 8135–8153, https://doi.org/10.1109/TNNLS.2022.3152527.

[39] S. Fan, J. Leng, Z. Feng, R. Lu, L. Dong, C. Lu, Dynamic control of bottom flash heat pump-assisted extractive distillation process for separating n-hexane and 1, 2-dichloroethane, Sep. Purif. Technol. 128830 (2024), https://doi.org/10.1016/j.seppur.2024.128830.

[40] G.F. Neto, K.D. Brito, R.P. Brito, Improving control of fully heat-integrated pressure swing distillation through partially flooded reboiler/condenser, Sep. Purif. Technol. 322 (2023) 124334, https://doi.org/10.1016/j.seppur.2023.124334.

[41] X. Zhang, C. Cui, H. Lyu, J. Sun, Integrated process design and self-optimizing control: a probabilistic approach, Chem. Eng. Sci. 286 (2024) 119667, https://doi.org/10.1016/j.ces.2023.119667.